Available at www.sciencedirect.com

ScienceDirect

journal homepage: www.elsevier.com/locate/he

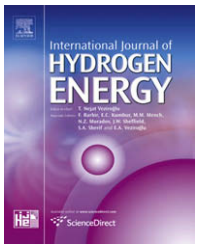

Iron molybdates as electrocatalysts for O_2 evolution reaction in alkaline solutions

R.N. Singh[a,*], Madhu[a], R. Awasthi[a], S.K. Tiwari[b]

[a]Department of Chemistry, Faculty of Science, Banaras Hindu University, Varanasi, U.P. 221005, India
[b]National Metallurgical Laboratory, Jamshedpur 831007, India

ARTICLE INFO

Article history:
Received 6 December 2008
Received in revised form
23 March 2009
Accepted 4 April 2009
Available online 5 May 2009

Keywords:
Iron molybdates
Oxygen evolution
Mixed oxides
Electrocatalysis
Current density

ABSTRACT

Iron molybdates with [Mo]/[Fe] ratios 1.0, 1.5 and 3.0 have been prepared by a co-precipitation method and produced in the form of thin films on a Ni support. These oxides follow the monoclinic crystal geometry. The study shows that the new oxide is highly active towards the oxygen evolution reaction in alkaline solutions and that its activity seems to depend upon the molar ratio of Mo and Fe in the oxide. The oxide with [Mo]/[Fe] = 1.0 is observed to exhibit the greatest electrocatalytic activity. The reaction order with respect to OH^- concentration has been found to be fractional (0.8–1.6). The Tafel slopes at low potentials were close to 35 mV.

1. Introduction

Electrochemical evolution and reduction of oxygen are of considerable interest owing to their use in many electrochemical devices such as secondary metal batteries, water electrolysis, chloralkali cells, fuel cells, electrosynthesis and metal electrowinning [1–5]. However, the oxygen reaction in aqueous solutions occurs at high overpotentials [5] resulting in substantial energy losses. To decline the oxygen overpotential, numerous electrocatalysts have been investigated and extensively reviewed [5–7]. Among the electrode materials investigated, transition metal mixed oxides belonging to spinel [8–17] and perovskite [18–22] families have been considered most promising, particularly in alkaline solutions and most extensively studied also [5–22].

Recently, we investigated [23] the physicochemical and electrochemical properties of a new type of mixed oxides with general formula, $MMoO_4$ (M = Co, Ni or Fe) towards O_2 evolution reaction (OER) in alkaline solutions. The oxides were prepared by thermal decomposition of mixed metal nitrates at 1123 K. The electrocatalytic activities of these oxides towards OER were found to be comparable to those of active cobalt-based spinel-type oxides, recently reported in literature [9,11,16,23–25]. To improve the catalytic efficiency further, the oxides, $NiMoO_4$ and $CoMoO_4$ were also obtained by a co-precipitation method under controlled pH (~5) and temperature (~353 K) conditions [26] and investigated; details of results are reported elsewhere [27,28]. We have now prepared iron molybdates with [Mo]/[Fe] = 1.0, 1.5 and 3.0 by a slightly modified precipitation method (pH ≈ 2 and T ≈ 373 K) [29] and investigated them by cyclic and steady state voltammetries and electrochemical impedance spectroscopy (EIS). Iron molybdate catalysts have recently been referred as good heterogonous catalysts for oxidation of methanol to

* *Corresponding author*. Tel.: +91 542 26701596; fax: +91 542 2368127.
E-mail address: rnsbhu@rediffmail.com (R.N. Singh).
0360-3199/$ – see front matter © 2009 International Association for Hydrogen Energy. Published by Elsevier Ltd. All rights reserved.
doi:10.1016/j.ijhydene.2009.04.006

formaldehyde [29]. Further, the catalytic behavior of iron molybdate is known to depend mainly on their Mo/Fe atomic ratio. The study of OER on iron molybdates, to our knowledge, has not been reported in literature. The present report describes the results of the study of OER on these new electrode materials.

2. Experimental

2.1. Preparation of catalyst

Iron molybdates with [Mo]/[Fe] = 1, 1.5, 3.0 were prepared by co-precipitation from a mixed aqueous solution of iron nitrate (Merck) and ammonium hepta molybdate (Merck), as described elsewhere [29]. For preparation of the oxide, Mo solution was first acidified (pH ~2) with HNO_3 and to this add iron nitrate solution slowly with vigorous stirring. After the completion of the iron nitrate solution addition, the precipitate was ripened in contact with mother liquor at 373 K for 1½ h under stirred condition, filtered, dried overnight at 393 K and finally calcined at 648 K for 10 h.

2.2. Characterization of oxide

X-ray diffraction of the oxide catalysts was recorded at a sweep rate of 2° min^{-1} on an X-ray diffractometer (Rigaku DMAX III) using Cu Kα as radiation source ($\lambda = 1.542$ Å). A Varian FTIR spectrophotometer (Model 3100) was used for recording the IR spectra. The average particle size of powders of the oxide, which were used for preparation of oxide electrodes, was measured using a particle size and shape analyzer ANKERSMID, Holland. Morphology of the compound has been studied by a scanning electron microscope (JEOL, 840A, Japan).

2.3. Oxide film electrode preparation

The oxide powders were obtained in the form of film on a nickel support through an oxide ink coatings. Prior to use, the support (1.5 × 1 cm) was etched for 20 min in conc. HCl, washed with double distilled water, degreased in acetone, cleaned ultrasonically in double distilled water, and then dried in air. The ink was made by mixing ~20 mg oxide powder with 0.6 ml propanol, 0.3 ml double distilled water and 2 drops nafion solution (1 wt%) and by subsequent ultrasonication of the mixture for 15 min. The ink, thus prepared, was dropped on the pretreated Ni-plate with the help of a syringe to cover the whole plate uniformly. The ink coated Ni-plate was then dried at 353 K for ½ h in an electrical furnace. Electrical contact with the oxide films was made as described previously [20].

2.4. Electrochemical studies

A three electrode single-compartment Pyrex glass cell was used to carry out electrochemical investigations. The reference and auxiliary electrode were Hg/HgO/1 M KOH ($E = 0.098$ V vs SHE) and pure Pt-foil (~8 cm^2), respectively. Values of the potential mentioned in the text are given against the Hg/HgO/1 M KOH electrode only.

The electrochemical impedance spectroscopy (EIS) study of the oxide film electrodes in 1 M KOH has been carried out with an ac voltage amplitude of 10 mV using an electrochemical impedance system (EG &G, PAR) provided with a lock-in-amplifier (Model 273A) and P-4 HP computer. The frequency range used in the study was 0.02–20 × 10^3 Hz and softwares employed were 'Power Sine' and 'ZsimpWin' version 3.00. 'M 352 Corrosion' software was used to perform the anodic Tafel polarization, details of which have already been described elsewhere [17].

3. Result and discussion

3.1. Structural and surface characterization

3.1.1. IR spectra of oxide catalyst

IR spectra of the oxide catalysts, in the region 1200–400 cm^{-1}, shown in Fig. 1 demonstrate a strong broad band at 850–842 cm^{-1} and a weak band at ~961 cm^{-1} which can be assigned to respectively tetrahedric species of Mo in $Fe_2(MoO_4)_3$ and Fe–O–Mo bond vibrations [29]. Further, the oxides with [Mo]/[Fe] = 1.5 and 3.0 exhibit two characteristic IR bands of MoO_3, a weak at ~995 cm^{-1} and a strong and broad one at 608–630 cm^{-1} [29], while these bands are absent in the IR spectrum of the compound with Mo/Fe atomic ratio 1.0. Furthermore, IR spectra of compounds with [Mo]/[Fe] = 1.5 and 3.0 show a weak band at 477–480 cm^{-1} which can be ascribed to Fe–O–Mo stretching vibration mode.

3.1.2. X-ray diffraction

Fig. 2 shows the X-ray diffraction of the oxides with [Mo]/[Fe] = 1, 1.5 and 3.0 recorded between $2\theta = 20°$ and $2\theta = 80°$. This figure demonstrates that the present co-precipitation method yields almost pure crystalline oxide, $Fe_2(MoO_4)_3$ with [Mo]/[Fe] = 1.5, however, the other two oxides with [Mo]/[Fe] = 1.0 and 3.0 contain impurities of mainly Fe_2O_3 ($2\theta = 24.14°$ & $d = 3.784$ Å; $2\theta = 33.16°$ & $d = 2.699$ Å and $2\theta = 54.11°$ & $d = 1.694$ Å) and

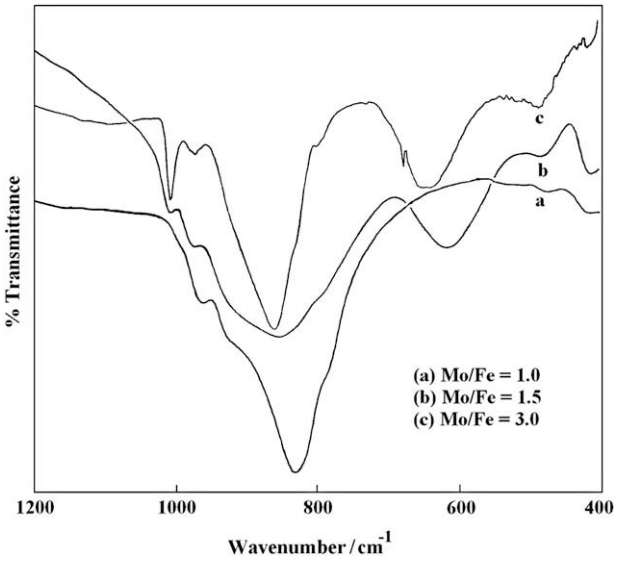

Fig. 1 – IR spectrum of $Fe_2(MoO_4)_3$ sintered at 648 K for 10 h.

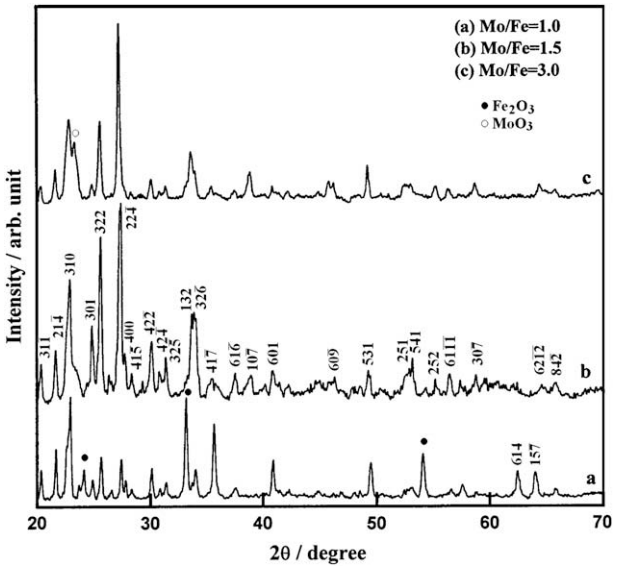

Fig. 2 – XRD of $Fe_2(MoO_4)_3$ sintered at 648 K for 10 h.

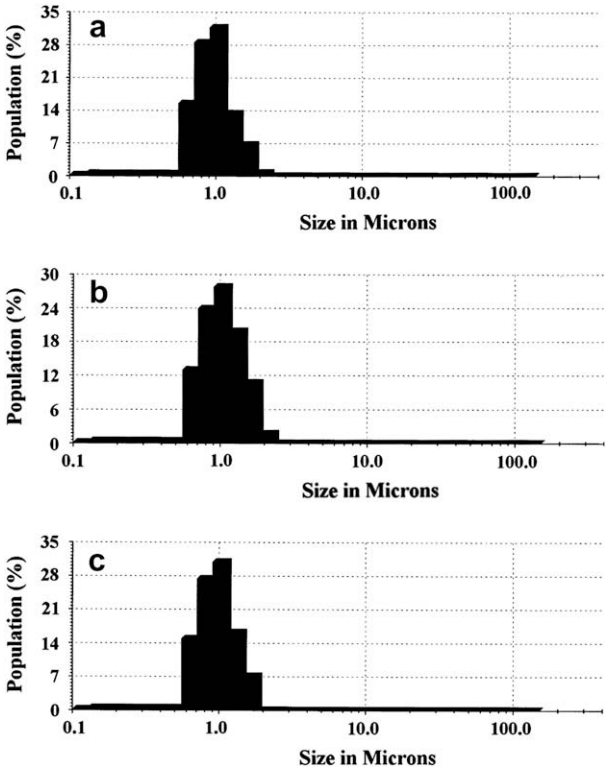

Fig. 3 – A typical histogram of particle size, based on area density of the $Fe_2(MoO_4)_3$. (a) [Mo]/[Fe] = 1.0, (b) [Mo]/[Fe] = 1.5 and (c) [Mo]/[Fe] = 3.0.

MoO_3 ($2\theta = 23.33°$ & $d = 3.81$ Å). The crystallites of oxides followed the monoclinic cell geometry. Values of the cell parameters (Table 1) were computed assuming $a \neq b \neq c$ and $\alpha = \gamma = 90°$ and $\beta \neq 90°$ and have been found to be very close to their respective literature values (JCPDS ASTM file no. 35-0183).

Value of the crystallite size (S) of oxides shown in Table 1 was estimated using the Scherrer formula [15]. The most intense X-ray peaks employed for estimation of S correspond to Bragg angles, 22.95 (310), 27.40 ($22\bar{4}$) and 27.24° ($22\bar{4}$) in the case of oxides with [Mo]/[Fe] = 1, 1.5 and 3, respectively. Table 1 shows that the crystallite size is the lowest with [Mo]/[Fe] ratio 1.5 and the largest with [Mo]/[Fe] = 3.0.

3.1.3. *Particle size/SEM*

The mean particle size of oxides has been determined using a particle size & shape analyzer. Histograms for particle size of powders of the oxides are shown in Fig. 3. As seen from the density curve Fig. 3 the particle size varies from 0.1 to 200 μ. The size range was divided into a number of segments and the average was calculated using the formula,

$$\text{average size based on length} = \sum x\,dN/\sum dN \text{ and}$$
$$\text{average size based on area} = \left(\sum x^2\,dN/\sum dN\right)^{1/2}$$

where x is the mean length of the segment and dN is the number of particles (% population) of size falling between that segment of size. The above statistical calculation was performed by the software of the analyzer.

Values of the mean particle size, based on both length and area density graphs, are given in Table 2. This table shows that both the area and length density graphs produce nearly the same values for the mean particle size, which, thereby, indicate that the oxide particles are nearly spherical in shape. In fact, this is found to be nearly true from scanning electron micrograph (SEM) of the oxide with [Mo]/[Fe] = 1.0 shown in Fig. 4.

3.2. *Electrochemical characterization*

3.2.1. *Cyclic voltammetry*

Fig. 5 shows cyclic voltammograms of iron molybdate/Ni electrodes in 1 M KOH at 298 K. Each curve in Fig. 5 shows an anodic ($E_{pa} \approx 465$ mV) and two cathodic peaks ($E_{pc} \approx 450$ mV & $E_{pc} \approx 380$ mV). Ni used as support for obtaining an oxide

Table 1 – Values of the cell parameters.

Oxide	a (Å)	b (Å)	c (Å)	β (degree)	S (nm)
$Fe_2(MoO_4)_3$ [Mo]/[Fe] = 1.0	15.70	9.34	18.20	125.60	~29
$Fe_2(MoO_4)_3$ [Mo]/[Fe] = 1.5	15.78	9.27	18.26	125.46	~21
$Fe_2(MoO_4)_3$ [Mo]/[Fe] = 3.0	15.70	9.40	18.30	125.60	~34

Table 2 – Mean particle size of catalyst powders.

Oxide	Mean particle size (μm)	
	Area based	Length based
$Fe_2(MoO_4)_3$ ([Mo]/[Fe] = 1.0)	0.87	0.79
$Fe_2(MoO_4)_3$ ([Mo]/[Fe] = 1.5)	0.95	0.90
$Fe_2(MoO_4)_3$ ([Mo]/[Fe] = 3.0)	0.88	0.84

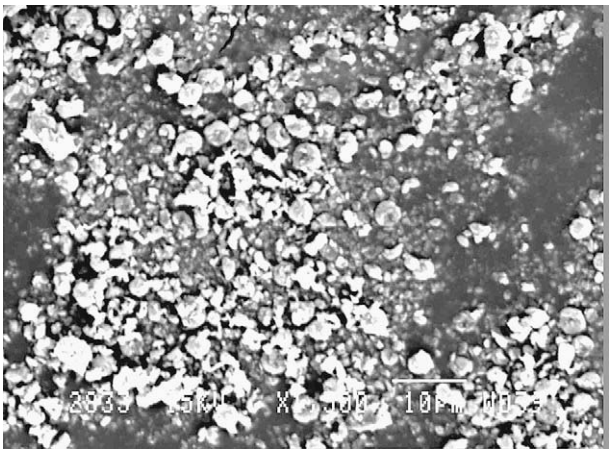

Fig. 4 – SEM picture of $Fe_2(MoO_4)_3$ ([Mo]/[Fe] = 1.0) at a magnification: ×1500.

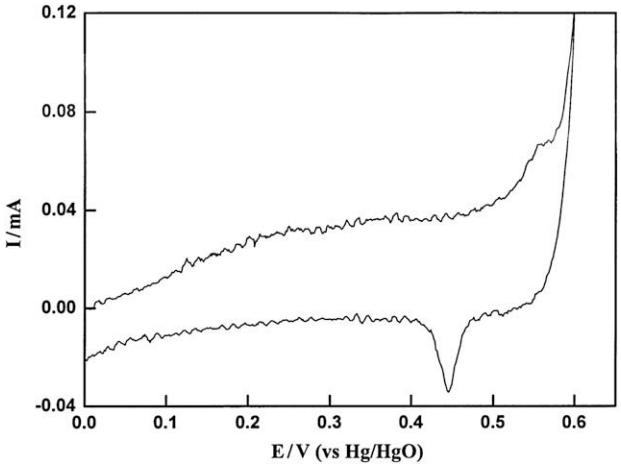

Fig. 6 – A cyclic voltammograms of $Fe_2(MoO_4)_3$ ([Mo]/[Fe] = 1.0)/Pt electrode at the scan rate of 50 mV s^{-1} in 1 M KOH at 298 K.

electrode is known to undergo the oxidation–reduction ($Ni^{2+} \rightarrow Ni^{3+}$) reaction during the anodic cycling condition due to the electrolyte contact [30]. In order to ascertain the contribution of Ni substrate, if any, the cyclic voltammogram of the iron molybdate ([Mo]/[Fe] = 1.0) film on Pt was recorded under similar experimental condition, and the result, so obtained, indicates (Fig. 6) only one anodic ($E_{pa} \approx 550$ mV) and one corresponding cathodic ($E_{pc} \approx 445$ mV) peak. As the Pt substrate does not exhibit any oxidation or reduction peak under the employed experimental conditions, the observed pair of redox peaks must has been produced due to the oxidation–reduction of the oxide overlayer only. Therefore, the observed pair of anodic ($E_{pa} \approx 465$ mV) and cathodic peak ($E_{pc} \approx 380$ mV) in CV of the oxide/Ni electrodes has been originated from the oxidation–reduction of the Ni substrate due to the electrolyte contact. On the other hand, the observed pair of redox peaks ($E_{pa} \approx 550$ and $E_{pc} \approx 445$ mV) for the oxide film on Pt indicates the transformation of low valence Fe(III) species in the surface film into its higher valence, mainly Fe(VI) species. This transformation is plausible based on the Pourbaix diagram of Fe. However, the anodic peak corresponding to the oxidation of iron molybdate film on Ni (Fig. 5) is not very clear and it appears in the form of a shoulder ($E = 530$–550 mV) just prior to the onset of oxygen evolution. Thus, the observed anodic shoulder at $E \approx 540$ mV and a cathodic peak at $E \approx 450$ mV for the oxide films on Ni have been produced as a result of the formation of a similar redox couple, as observed at the Pt/oxide ([Mo]/[Fe] = 1.0) electrode (Fig. 6). Further, the observed anodic shoulder shifts from 530 to 550 mV towards the O_2 evolution region with an increase in [Mo]/[Fe] ratio from 1.0 to 3.0.

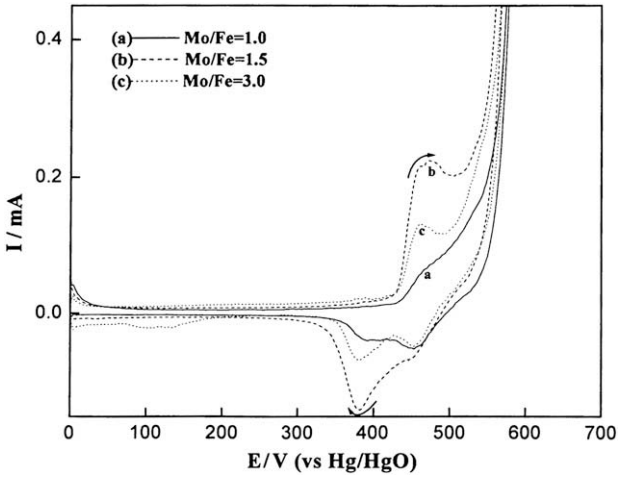

Fig. 5 – Cyclic voltammograms of $Fe_2(MoO_4)_3$/Ni electrodes at the scan rate of 50 mV s^{-1} in 1 M KOH at 298 K.

3.2.2. *Electrochemical impedance spectroscopy*

In order to determine the electrochemical active area vis-à-vis kinetics of OER, the EIS study has been carried out on the oxide electrodes at varying potentials chosen in the potential range, 0.55–0.64 V, in 1 M KOH. The potentials chosen for the study belong to the initial region of the OER. Before recording each spectrum, the electrode was first kept at the applied potential to equilibrate for 300 s. EIS spectra obtained are shown in Fig. 7. This figure indicates the formation of a large semicircle at the intermediate and low frequencies, the diameter of which decreases with increasing the potential. The decrease in the diameter at higher potentials can be attributed to the increase in the rate of the OER [31]. At high frequencies, each spectrum shown in Fig. 7 indicates the formation of a potential independent arc.

Experimental impedance data obtained on each electrocatalyst were simulated by using a common and best-fit electrical equivalent circuit, as shown in Fig. 8a.

The circuit description code for this proposed model is $R_s(R_1Q_1)$ (R_2Q_2). The parallel (R_1Q_1) combination describes the properties of the oxide in the bulk, while the parallel (R_2Q_2) combination is associated with the OER. Symbol R_s represents the solution resistance, R_1 and R_2 represent the oxide film resistance (Ω) and the charge transfer resistance and Q_1 and Q_2 represent the constant phase element for the bulk oxide and the oxide–solution interfaces respectively. Based on the

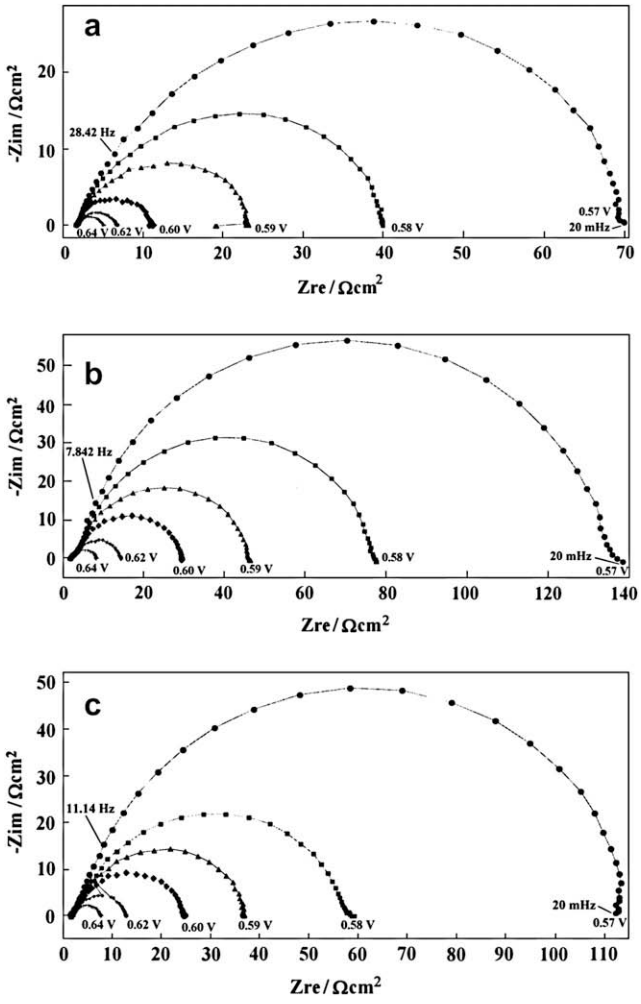

Fig. 7 – Complex impedance diagrams for $Fe_2(MoO_4)_3$/Ni electrodes in 1 M KOH at varying potentials; (a) [Mo]/[Fe] = 1.0, (b) [Mo]/[Fe] = 1.5 and (c) [Mo]/[Fe] = 3.0.

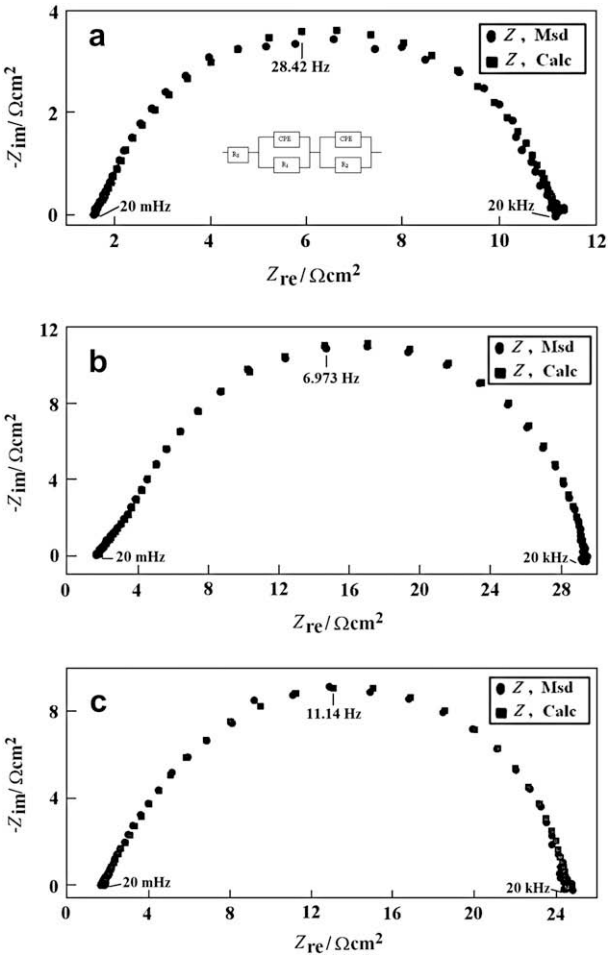

Fig. 8 – Nyquist plots (experimental and simulated) for $Fe_2(MoO_4)_3$/Ni electrodes at 0.62 V in 1 M KOH; (a) [Mo]/[Fe] = 1.0, (b) [Mo]/[Fe] = 1.5 and (c) [Mo]/[Fe] = 3.0.

proposed circuit model, the EIS spectrum obtained agrees reasonably well with the experimental curve. Simulated and experimental curves in Nyquist model are given at $E = 0.62$ V in Fig. 8. Estimates of the circuit parameters are given in Table 3.

The C_{dl} values given in Table 3 have been estimated using the following equation

$$Q_2 = (C_{dl})^n \left[(R_s)^{-1} + (R_{ct})^{-1}\right]^{1-n} \quad (1)$$

The above equation was given by Brug et al. [32] and used to estimate the C_{dl} when the CPE is coupled, as in the present case, with the charge transfer resistance. The electrochemically active surface area/roughness factor (R_F) of electrocatalysts has been estimated using the relation [19,20],

$$R_F = \text{Observed } C_{dl} \text{ of the oxide electrode} / C_{dl} \text{ of the smooth oxide surface } (60\ \mu\text{Fcm}^{-2})$$

Table 3 shows that the magnitude of R_2 decreases and hence the rate of the OER increases with the increase in potential. Further, the roughness of the oxide catalysts seems to be independent of the applied potential in the O_2 evolution region. This shows that the nature of the oxide surface does not change practically with the applied potential in the oxygen evolution region. It is considered that in the O_2 evolution region, the oxide electrode is enveloped by a layer of adsorbed OH^- ions. Thus, the latter layer of adsorbed OH^- ions becomes in direct contact with OH^- ions in bulk and not the oxide layer. Further, the adsorbed OH^- ions might be under an adsorption maximum condition due to lateral interaction among adsorbed OH^- ions [18]. Therefore, the capacitance and hence the relative roughness of the electrode do not change practically with E.

Based on values of the R_2 at a constant potential (E), the electrocatalytic activity of the electrocatalyst with [Mo]/[Fe] = 1 is the greatest one. However, the average R_F value for this electrode is the lowest among all the three electrodes. Thus, the enhanced electrocatalytic activity of the electrode towards the OER may be ascribed to the improvement in the electronic properties of the material. The average relative R_F value for the oxide was estimated by taking average of all the R_F values, excepting marked by an asterisk (Table 3), determined in the potential region,

Table 3 – Values of the equivalent circuit parameters for iron molybdates in 1 M KOH.

Electrode	E (V)	R_s ($\Omega\,cm^{-2}$)	R_1 ($\Omega\,cm^{-2}$)	$Q_1 \times 10^3$ ($S\,s^n\,cm^{-2}$)	n_1	$\tau_1 \times 10^3$	R_2 ($\Omega\,cm^{-2}$)	$Q_2 \times 10^3$ ($S\,s^n\,cm^{-2}$)	n_2	$\tau_2 \times 10^1$	$C_{dl} \times 10^3$ ($F\,cm^{-2}$)	R_F
$Fe_2(MoO_4)_3$	0.55	1.86	48.9	3.57	0.74	93.1	202.6	1.72	0.95	3.30	1.27	~21*
Mo/Fe = 1.0	0.57	1.69	0.15	0.28	1.00	0.04	69.34	1.55	0.82	0.70	0.42	~7
	0.59	1.64	0.20	0.46	0.97	0.06	21.51	1.60	0.83	0.20	0.45	~8
	0.60	1.58	0.13	0.43	1.00	0.05	9.46	1.63	0.83	0.07	0.47	~8
	0.62	1.83	0.07	0.94	1.00	0.07	4.79	2.05	0.78	0.03	0.40	~7
	0.64	1.82	0.08	1.05	1.00	0.08	3.15	2.01	0.80	0.02	0.45	~7
$Fe_2(MoO_4)_3$	0.55	1.74	4.03	4.16	0.59	0.44	496.3	1.25	0.94	6.00	0.84	~14
Mo/Fe = 1.5	0.57	1.67	3.39	4.51	0.60	0.97	129.9	1.33	0.93	1.50	0.82	~14
	0.59	1.62	3.32	6.1	0.60	1.40	41.24	1.41	0.93	0.50	0.88	~15
	0.6	1.63	2.88	5.85	0.61	1.22	24.8	1.48	0.92	0.30	0.90	~15
	0.62	1.64	2.68	6.51	0.61	1.31	9.92	1.63	0.92	0.10	0.98	~16
	0.64	1.68	2.05	5.59	0.63	0.82	4.41	1.64	0.94	0.05	1.11	~19*
$Fe_2(MoO_4)_3$	0.55	1.55	6.08	1.22	0.54	7.93	492.00	0.95	0.92	4.40	0.55	~9
Mo/Fe = 3.0	0.57	1.67	3.39	4.52	0.60	0.97	129.9	1.33	0.93	1.50	0.82	~14
	0.59	1.76	2.18	4.56	0.71	1.48	33.08	1.13	0.89	0.30	0.55	~9
	0.6	1.75	2.34	5.98	0.68	1.89	20.46	1.16	0.91	0.20	0.61	~10
	0.62	1.64	2.68	6.51	0.61	1.31	9.92	1.63	0.92	0.10	0.98	~16
	0.64	1.79	0.26	0.53	0.97	0.11	5.03	1.21	0.86	0.03	0.42	~7*

0.55–0.64 V; average values were 7.4 ± 0.5, 15 ± 1, and 12 ± 3 for the oxides with 1.0, 1.5, and 3.0, respectively.

Values of the apparent current density (j) at varying potentials were also estimated using the relation,

$$R_{ct} = RT/nFj$$

where R, T, n, F, and j are the molar gas constant ($J\,mol^{-1}\,K^{-1}$), temperature (K), no. of electrons involved in the reaction which is 4 in the present case, Faraday constant and the apparent current density ($A\,cm^{-2}$), respectively. The j–E data, thus obtained, were expressed in form of the Tafel plot as shown in Fig. 9, which is found to be linear with a slope of ~40 mV for the OER on iron oxide electrode.

3.2.3. *Activity test*

The catalytic activity of the oxide film electrode towards the OER was determined by recording the iR_s-compensated Tafel polarization curves (E vs $\log j$) at a slow scan rate ($0.2\,mV\,s^{-1}$) in 1 M KOH at 298 K (Fig. 10) . The iR_s was automatically compensated at an interval of 10 s using the current interrupt technique provided in electrochemical impedance system. Each E vs $\log j$ curve in Fig. 10 displays two apparent Tafel slopes, one at low (~35 mV) and the other (67–70 mV) at higher potentials. Nearly the same Tafel slope values for all the three electrodes indicate a similar mechanism for the OER. To compare the catalytic activities of electrocatalysts, the oxygen evolution apparent current densities at two constant potentials, 0.60 and 0.65 V were noted from Fig. 10 and values are given in Table 4.

The reaction order with respect to [OH^-] has also been determined by carrying out polarization experiment at varying KOH concentrations, maintaining the ionic strength ($\mu = 2.0$) of the medium constant. With the help of these curves, the linear $\log j$ vs $\log$ [OH^-] plots were constructed at

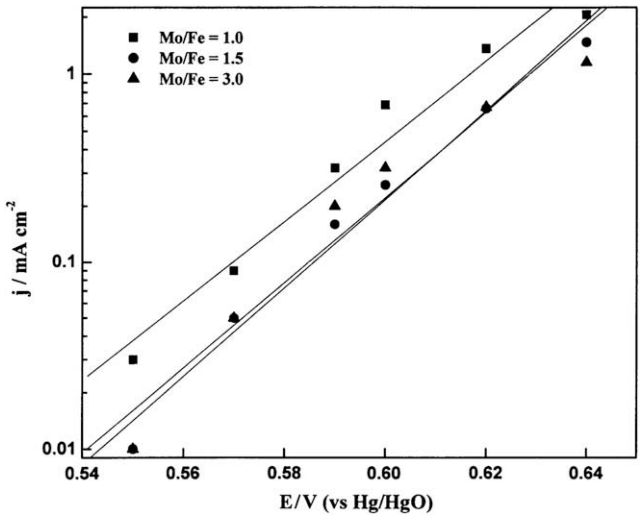

Fig. 9 – E vs $\log j$ plot for $Fe_2(MoO_4)_3$ electrodes derived from impedance data.

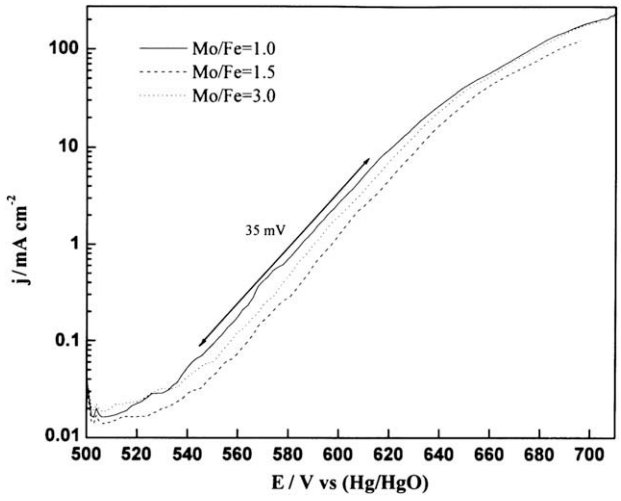

Fig. 10 – Tafel plot for O_2 evolution on $Fe_2(MoO_4)_3$ electrodes in 1 M KOH.

Table 4 – Values of the electrode kinetic parameters for oxygen evolution on iron molybdates in 1 M KOH at 298 K.

$Fe_2(MoO_4)_3$ where Mo/Fe	Loading (mg/cm^2)	Tafel slope (mV)		Order (p)	E (mV) at i (mA/cm^2)		i (mA/cm^2) at E (mV)	
		b_1	b_2		10	100	600	650
1.0	1.50 ± 0.2	~35	~67	1.6	618 ± 3	674 ± 5	2.70	41.22
1.5	1.68 ± 0.3	~35	~70	0.8	630 ± 1	685 ± 3	1.28	29.02
3.0	1.55 ± 0.2	~35	~69	1.5	627 ± 1	678 ± 1	1.80	36.50

a constant potential as shown in Fig. 11 and the order was then determined by measuring the slope of these straight lines. Values of the reaction order, thus determined, were ~1.6, ~0.8 and ~1.5 for the oxide with [Mo]/[Fe] = 1, 1.5 and 3.0, respectively. For determination of the order, the first linear region of the E vs log j curves was considered.

Results shown in Table 4 demonstrate that the apparent electrocatalytic activity of the oxide electrode with [Mo]/[Fe] = 1 is the greatest one. It is also greater than those recently reported for $NiMoO_4$ [27] and $CoMoO_4$ [28] under identical experimental conditions. Also, on normalizing the apparent current densities of electrodes by their respective electrochemically active areas (i.e. roughness), the oxide catalyst with [Mo]/[Fe] = 1 shows the highest electrocatalytic activity. Values of the true current density ($j_t = j/R_F$, where R_F being the average oxide roughness obtained by EIS) of the oxides with [Mo]/[Fe] = 1.0, 1.5 and 3.0 were 5.7 ± 0.4, 1.9 ± 0.2 and 3.0 ± 0.8 mA cm^{-2} at $E = 0.650$ V in 1 M KOH at 298 K, respectively. On the other hand, under similar experimental conditions, the electrodes, $NiMoO_4$ ($j_t = 2.9 \times 10^{-3}$ mA cm^{-2}, $R_F \approx 1165$) and $CoMoO_4$ ($j_t = 9.3 \times 10^{-3}$ mA cm^{-2}, $R_F \approx 817$) produced relatively low j_t compared to the oxide catalysts of the present study.

The CV study shows that in the case of iron molybdate, the electroformation of O_2 takes place at the oxidized Fe(VI) site, while that in case of $NiMoO_4$ and $CoMoO_4$, on Ni(III) and Co(IV) sites, respectively. As the active Fe(VI) (d^2) site is highly d-electron deficient ion compared to sites, Co(IV) (d^5) and Ni(III) (d^7), it would facilitate the oxidation process more strongly than Ni(III) or Co(IV) site.

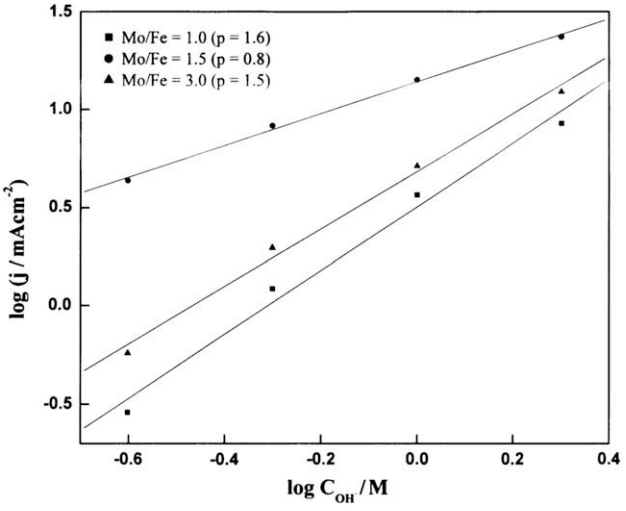

Fig. 11 – log j vs log [OH^-] plot for O_2 evolution of $Fe_2(MoO_4)_3$/Ni electrodes at a constant potential (0.590 V).

The apparent electrocatalytic activities of the new electrodes, $Fe_2(MoO_4)_3$ with [Mo]/[Fe] = 1, 1.5, and 3.0 towards O_2 evolution are found to be comparable and even better to those of active Co-based spinel-type electrodes recently reported in literature. For instance, Chi et al. [24] observed j = ~162–290 mA cm^{-2} at $E = 0.70$ V vs SCE (= ~0.844 V vs Hg/HgO) on $ZnCo_2O_4$ deposited on Ni by electrophoretic deposition method in 1 M KOH. Hamdani et al. [25] found $j = 16$ mA cm^{-2} at $E = 0.80$ V vs SCE (= ~0.944 V vs Hg/HgO) on Li-(10%) doped Co_3O_4 on glass obtained by spray pyrolysis. Svegl et al. [11] found $j = 100$ mA cm^{-2} at $E \approx 0.640$ (= ~0.740 V vs Hg/HgO) and 0.715 V vs Ag/AgCl (= ~0.815 V vs Hg/HgO) for sol–gel derived Co_3O_4 (773 K) and Li-doped Co_3O_4 (773 K) films on Pt, respectively, while the same films on ITO/glass substrate displayed a relatively low activity. Tavares et al. [9] prepared catalytic films of $NiCo_2O_4$ on Ni by thermal decomposition of aqueous nitrate solutions and found $E = 0.65$ V vs Hg/HgO corresponding to j ~ 68 mA cm^{-2} in 5 M KOH.

The observed b and p values for the OER on these new catalyst systems are in fair agreement with those recently reported for similar films of $MMoO_4$ (M = Co, Fe or Ni) (b_1 = 37–44 mV, b_2 = 54–73; p = 1.2–1.9) [23], $CoFe_{2-x}Cr_xO_4$ (b_1 = 40–51, b_2 = 60–89 mV; p = 1.2–1.4) [16], and $MnFe_{2-x}Cr_xO_4$ (b = 40 mV; p = 1.8) [12]. Similar values of the Tafel slopes were also found on $CuCo_2O_4$ films (b = 40 mV) on Ni and on $LaPO_4$-bonded Ni (obtained by the thermal decomposition of the metal nitrates) [14,15].

4. Conclusions

The study demonstrates that the electrocatalytic activity of iron molybdate towards OER depends upon the molar ratio of Mo and Fe in the oxide. The oxide with [Mo]/[Fe] = 1.0 is found to display the greatest electrocatalytic activity. Values of Tafel slope for OER determined by the anodic polarization and impedance techniques match excellently. The catalytic activity of these oxides for OER is comparable to those of active cobalt-based spinel electrodes.

Acknowledgements

Authors thank the CSIR for the financial support of the work through a research project (Ref. No. 01(2033)/06/EMR-II). One of the authors (Madhu) also thank the University Grants Commission (UGC), Government of India for the award of 'Rajiv Gandhi National Fellowship' to carry out the investigation.

REFERENCES

[1] Chebotareva N, Nyokong T. First-row transition metal phthalocyanines as catalysts for water electrolysis: a comparative study. Electrochim Acta 1997;42:3519–24.

[2] Vielstich W. Electrochemical energy conversion – methanol fuel cell as example. Braz J Chem Soc 2003;14:503–9.

[3] Mao L, Zhang D, Sotomura T, Nakatsu K, Koshiba N, Ohsaka T. Mechanistic study of the reduction of oxygen in air electrode with manganese oxides as electrocatalysts. Electrochim Acta 2003;48:1015–21.

[4] Huang H, Zhang W, Li M, Gan Y, Chen J, Kuang Y. Carbon nanotubes as a secondary support of a catalyst layer in a gas diffusion electrode for metal air batteries. J Colloid Interface Sci 2005;284:593–9.

[5] O'Sullivan EJM, Calvo EJ. Reaction at metal oxide electrodes. In: Compton RG, editor. Comprehensive chemical kinetics: electrode kinetics reactions, vol. 27. Amsterdam Elsevier; 1987. p. 247–360.

[6] Trasatti S, Lodi G. Oxygen and chlorine evolution at conductive metallic oxide anodes. In: Trasatti S, editor. Electrodes of conductive metallic oxides, part B. Amsterdam: Elsevier; 1981. p. 521–625.

[7] Trasatti S. Transition metal oxides: versatile materials for electrocatalysis. In: Lipkowski J, Ross PN, editors. Electrochemistry of novel materials. New York: VCH; 1994. p. 207–95.

[8] Tavares AC, Bochatay L, da Silva Pereira MI, da Costa FMA. Oxygen evolution on $NiCo_{2-x}Rh_xO_4$ spinel system. Electrochim Acta 1996;41:1953–9.

[9] Tavares AC, Cartaxo MAM, da Silva Pereira MI, Costa FM. Effect of the partial replacement of Ni or Co by Cu on the electrocatalytic activity of the $NiCo_2O_4$ spinel oxide. J Electroanal Chem 1999;464:187–97.

[10] Rios E, Gautier J-L, Poillerat G, Chartier P. Mixed valency spinel oxides of transition metals and electrocatalysis: case of the $Mn_xCo_{3-x}O_4$ system. Electrochim Acta 1998;44:1491–7.

[11] Svegl F, Orel B, Grabec-Svegl I, Kaucic V. Characterization of spinel Co_3O_4 and Li-doped Co_3O_4 thin film electrocatalysts prepared by the sol–gel route. Electrochim Acta 2000;45: 4359–77.

[12] Singh RN, Singh JP, Nguyen Cong H, Chartier P. Effect of partial substitution of Cr on electrocatalytic properties of $MnFe_2O_4$ towards O_2-evolution in alkaline medium. Int J Hydrogen Energy 2006;31:1372–8.

[13] Laouini E, Hamdani M, Pereira MIS, Douch J, Mendonca MH, Berghoute Y, et al. Preparation and electrochemical characterization of spinel type Fe–Co_3O_4 thin film electrode in alkaline medium. Int J Hydrogen Energy 2008;33:4936–44.

[14] Fatih K, Marsan B. $Cu_xCo_{3-x}O_4$/$LaPO_4$-bonded Ni electrodes for oxygen evolution in alkaline solution: preparation, physicochemical properties and electrochemical behavior. Can J Chem 1997;75:1597–607.

[15] Fradette N, Marsan B. Surface studies of $Cu_xCo_{3-x}O_4$ electrodes for the electrocatalysis of oxygen evolution. J Electrochem Soc 1998;145:2320–7.

[16] Singh RN, Singh NK, Singh JP. Electrocatalytic properties of new active ternary ferrite film anodes for O_2 evolution in alkaline medium. Electrochim Acta 2002;47:3873–9.

[17] Singh RN, Singh JP, Lal B, Thomas MJK, Bera S. New $NiFe_{2-x}Cr_xO_4$ spinel films for O_2 evolution in alkaline solutions. Electrochim Acta 2006;51:5515–23.

[18] Bockris JO'M, Otagawa T. Mechanism of oxygen evolution on perovskites. J Phys Chem 1983;87:2960–71.

[19] Bockris JO'M, Otagawa T. The electrocatalysis of oxygen evolution on perovskites. J Electrochem Soc 1984;131: 290–302.

[20] Tiwari SK, Chartier P, Singh RN. Preparation of perovskite-type oxides of cobalt by the malic acid aided process and their electrocatalytic surface properties in relation to oxygen evolution. J Electrochem Soc 1995;142:148–53.

[21] Singh RN, Lal B. High surface area lanthanum cobaltates and its A and B site substituted derivatives for electrocatalysis of O_2 evolution in alkaline solution. Int J Hydrogen Energy 2002; 27:45–55.

[22] Lal B, Raghunandan MK, Gupta M, Singh RN. Electrochemical behaviour of perovskite-type $La_{1-x}Sr_xCoO_3$ ($0 \le x \le 0.4$) obtained by a novel stearic acid sol–gel method for electrocatalysis of O_2 evolution in KOH solutions. Int J Hydrogen Energy 2005;30:723–9.

[23] Singh RN, Singh JP, Singh A. Electrocatalytic properties of new spinel-type $MMoO_4$ (M = Fe, Co & Ni) electrodes for oxygen evolution in alkaline solutions. Int J Hydrogen Energy 2008;33:4260–4.

[24] Chi B, Jianbao L, Xiaozhan Y, Hong L, Ning W. Electrophoretic deposition of $ZnCo_2O_4$ spinel and its electrocatalytic properties for oxygen evolution reaction. Electrochim Acta 2005;50:2059–64.

[25] Hamdani M, Pereira MIS, Douch J, Ait Addi A, Berghoute Y, Mendonca MH. Physicochemical and electrocatalytic properties of Li–Co_3O_4 anodes prepared by chemical spray pyrolysis for application in alkaline water electrolysis. Electrochim Acta 2004;49:1555–63.

[26] Brito JL, Barbosa AL. Effect of phase composition of the oxidic precursor on the HDS activity of the sulfided molybdates of Fe(II), Co(II), and Ni(II). J Catal 1997;171:467–75.

[27] Singh RN, Madhu, Awasthi R, Sinha ASK. Preparation and electrochemical characterization of a new $NiMoO_4$ catalyst for electrochemical O_2 evolution. J Solid State Electrochem, in press. doi:10.1007/s10008-008-0744-7.

[28] Singh RN, Madhu, Awasthi R, Sinha ASK. Electrochemical characterization of a new binary oxide of Mo with Co for O_2 evolution in alkaline solution. Electrochim Acta 2009;54: 3020–5.

[29] Soares APV, Farinha Portela M, Kiennemann A, Hilarie L, Millet JMM. Iron molybdate catalysts for methanol to formaldehyde oxidation: effects of Mo excess on catalytic behaviour. Appl Catal A Gen 2001;206:221–9.

[30] Singh RN, Singh JP, Singh NK, Lal B, Chartier P, Koening JF. Sol–gel derived spinel $M_xCo_{3-x}O_4$ (M = Ni, Cu; $0 \le x \ge 1$) films and oxygen evolution. Electrochim Acta 2000;45:1911–9.

[31] Palmas S, Ferrara F, Vacca A, Mascia M, Polcaro AM. Behaviour of cobalt oxide electrodes during oxidative processes in alkaline medium. Electrochim Acta 2007;53: 400–6.

[32] Brug GJ, Van den Eeden ALG, Rehbach MS, Sluyters JH. The analysis of electrode impedances complicated by the presence of a constant phase element. J Electroanal Chem 1984;176:275–95.